Since January 2020 Elsevier has created a COVID-19 resource centre with free information in English and Mandarin on the novel coronavirus COVID-19. The COVID-19 resource centre is hosted on Elsevier Connect, the company's public news and information website.

Radiation Physics and Chemistry 177 (2020) 109169

Contents lists available at ScienceDirect

Radiation Physics and Chemistry

journal homepage: www.elsevier.com/locate/radphyschem

Calculations of energy deposition and ionization in the 2019 novel coronavirus by electron beam irradiation

Xiaqi Zhang, Fang Wang, Ming Weng, Meng Cao*

Key Laboratory for Physical Electronics and Devices, Ministry of Education, School of Electronic Science and Engineering, Xi'an Jiaotong University, Xi'an, Shaanxi, 710049, China

ARTICLE INFO

Keywords:
Electron irradiation
Energy deposition
Ionization

ABSTRACT

Using Monte Carlo methods, this study investigates energy deposition of energetic electrons and ionization in the 2019 novel coronavirus by electron irradiation, which are important characteristic quantities related with biological damage formation. The inelastic scattering of low-energy electrons (< 10 keV) was calculated by dielectric theory. The optical energy-loss functions of viral proteins and RNA were derived from an empirical method in the energy-loss range < 40 eV and the calculation of optical parameters of the biomolecules. The densities and distributions of energy deposition and ionization were calculated from the stopping power and inelastic cross-sections in the electron-cascade simulation. Electrons with primary energies of approximately 1–3 keV produced significant energy deposition and ionization in the target coronavirus. More energetic electrons were less effective due to the larger electron range and fewer scattering events in the coronavirus.

1. Introduction

The 2019 novel coronavirus (2019-noCoV) was responsible for the COVID-19 pandemic of 2020 (Sohrabi et al., 2020; WHO World Health Organization, 2020). To avoid exposure to COVID-19, effective methods that kill or inactivate the virus on contaminated media or in specific environments are demanded. Electron beam irradiation is widely used for killing microorganisms, bacteria, and viruses (Berovic et al., 2002; Benson, 2002; Feng et al., 2020), because its penetration depth and dose can be controlled to comply with environmental protection requirements. Moreover, under controlled irradiation, the virus can be partially or totally inactivated, providing useful information on its properties (Lidzey et al., 1995; Smolko and Lombardo, 2005).

Electron irradiation damage on biological macromolecules is mainly characterized by inactivity and the irreversibly chain broken (Tan and Liu, 2014). The severity of these effects is highly correlated with the energy deposition and ionization in the molecules, which occur by inelastic interactions between the electrons and molecules (Boudaïffa et al., 2000; Kempner, 2001, 2011; Tan et al., 2018; Zhang and Tan, 2010). To properly understand electron irradiation effects on the novel coronavirus, the energy deposition and ionization must be calculated, because experimental evaluation with currently available methods is very difficult.

High-energy electrons (above tens of keV) are usually applied for antiseptic purposes. When primary electrons interact with a target molecule by inelastic scattering, they lose energy and excite the shell electrons as secondary electrons (SEs). Low-energy electrons, including decelerated primary electrons and SEs with energies below 50 eV, significantly contribute to the large number of SEs during the electron-cascade process, exerting a considerable ionization effect (Emfietzoglou et al., 2012; Nikjoo et al., 1997; Zhang and Tan, 2010). Therefore, the interaction of low-energy electrons with the main proteins and RNA macromolecules of the novel coronavirus was the key issue of our calculation. The stopping power was suitable for describing the energy-deposition probability in the target, and the ionization events were determined as the inelastic cross-sections of collisions with the shell electrons of an atom. The stopping power and ionization events of low-energy electrons are usually calculated by dielectric theory, which requires the energy-loss function (ELF). The ELF can be derived from the optical ELF (OELF) through a proper dispersion relation. However, as important input data for the calculation of the OELF, the optical parameters of macromolecules of proteins, RNA are not available. Tan et al. developed an empirical method that estimates the OELF of organic biomaterials at energy losses below 40 eV (Tan et al., 2004a, 2004b). The same approach is expected to be applicable to the novel coronavirus.

In this work, we calculated the distributions of energy deposition and ionization in the novel coronavirus irradiated with electrons having

* Corresponding author.
E-mail address: mengcao@mail.xjtu.edu.cn (M. Cao).

https://doi.org/10.1016/j.radphyschem.2020.109169
Received 2 June 2020; Received in revised form 20 August 2020; Accepted 29 August 2020
Available online 04 September 2020
0969-806X/

primary energies below 10 keV. The calculation was performed by Monte Carlo simulations of the electron cascade in the fundamental component macromolecules of the coronavirus, which are arranged in a multilayer spherical shell configuration. The distribution characteristics of the energy deposition and ionization were evaluated in each shell of the virus, and the influence of primary electron energy on the irradiation effects was determined. The characteristics of electron irradiation determined in this study can assist our understanding of irradiation-induced damage on the novel coronavirus.

2. Models and methods

2.1. Model of the coronavirus

For the calculations, we used a simplified physical model of the novel coronavirus with a multilayer spherical shell configuration. The model is based on published information of the novel coronavirus and similar known coronaviruses (CDC, 2020; Lu et al., 2020). The novel coronavirus is comparatively large (with an approximate diameter of 120 nm), and its main proteins are spiked glycoproteins (S) on the outer layer, envelope proteins (E) in the next layer, a water layer, the nucleocapsid (N), and RNA in the centre (see Fig. 1). The diameters of each shell are marked in Fig. 1. The components of each shell were assumed as the typical amino acid sequences or nucleobase sequences of the main proteins within the shell, extracted from the sequence resources published in the National Centre for Biotechnology Information (NCBI, 2020). The statistical results yielded the average molecular formulas of the three types of proteins as follows: $C_{4.95}H_{9.67}O_{2.49}N_{1.20}S_{0.04}$ for the spike proteins, $C_{5.23}H_{10.20}O_{1.25}N_{2.35}S_{0.04}$ for the envelope, and $C_{4.61}H_{9.29}O_{2.45}N_{1.30}S_{0.02}$ for the nucleocapsid. The RNA was determined as $C_{4.50}H_{4.68}O_{1.02}N_{3.67}$.

2.2. Calculation methods

The energetic electrons interact with the novel coronavirus through elastic and inelastic scattering. Elastic scattering describes the collision between electrons and the nuclei of the target atoms, which changes the direction of the electron trajectories. The elastic-scattering calculation of electrons with energy < 10 keV was usually based on the Mott cross-section. In this calculation, the atomic differential elastic-scattering cross-sections were taken from the NIST electron elastic-scattering cross-section database (Salvat et al., 2002). Following the additivity rule (Chiari et al., 2013; Jiang et al., 1997), the differential cross-section of each kind of molecule in the novel coronavirus was calculated by summing the differential cross-sections σ_{el} of the individual atoms in the target molecule as follows:

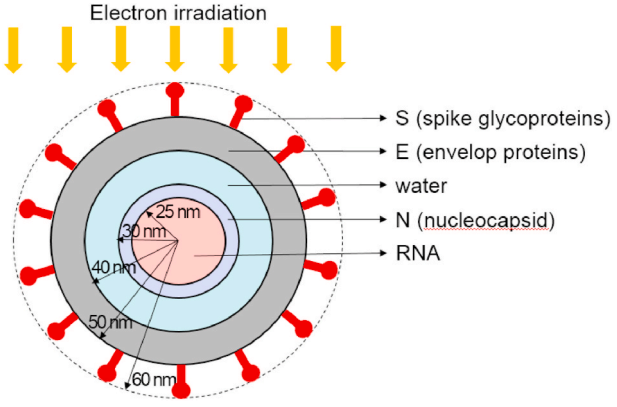

Fig. 1. Simplified structure of the 2019 novel coronavirus assumed in the present calculation, based on published information about the coronavirus (CDC, 2020; Lu et al., 2020; NCBI, 2020).

$$\frac{d\sigma_{el}(\theta)}{d\Omega} = \sum_i n_i \frac{d\sigma_{el-i}(\theta)}{d\Omega}, \tag{1}$$

where n_i is the atomic number of the i-th atom in the molecular formula, and Ω is the solid angle determined by the scattering angle θ.

The inelastic cross-sections of low-energy electrons are usually calculated by dielectric theory. This calculation requires the ELF, given by the negative of the reciprocal of the imaginary part of the dielectric function ($\mathrm{Im}[-1/\varepsilon(\mathbf{q}, \Delta E)]$). Penn (1987) and Ashley (1988) obtained the ELF by extending the dielectric function in the optical limit, where the momentum transfer is $\mathbf{q} = 0$. By fitting the OELF $\mathrm{Im}[-1/\varepsilon(0, \Delta E)]$ to the experimental optical data and introducing a suitable dispersion relation, the differential inelastic cross-section σ_{inel} of the incident electrons colliding with the shell electrons can be calculated as (Ashley, 1988)

$$\frac{d\sigma_{inel}(E, \Delta E)}{d\Delta E} = \frac{1}{2\pi a_0 N E}\mathrm{Im}\left[-\frac{1}{\varepsilon(0, \Delta E)}\right]L\left(\frac{\Delta E}{E}\right), \tag{2}$$

with

$$L(x) = (1-x)\ln\frac{4}{x} - \frac{7}{4}x + x^{3/2} - \frac{33}{32}x^2. \tag{3}$$

In these expressions, a_0 is the Bohr radius, N is the number of molecules per unit volume in the target, E is the electron energy, and ΔE is the energy transfer.

To calculate the energy loss along the electron trajectories, we require the stopping power of the electrons, which represents the average energy loss of an electron in the unit distance. The stopping power is given by

$$-\frac{dE}{ds} = \frac{1}{\pi a_0 E}\int_0^{E/2} \Delta E\,\mathrm{Im}\left[-\frac{1}{\varepsilon(0, \triangle E)}\right]G\left(\frac{\Delta E}{E}\right)d\Delta E, \tag{4}$$

where

$$G(x) = \ln\frac{1.1658}{x} - \frac{3}{4}x - \frac{x}{4}\ln\frac{4}{x} + \frac{1}{2}x^{3/2} - \frac{x^2}{16}\ln\frac{4}{x} - \frac{31}{48}x^2. \tag{5}$$

However, the experimental OELF data of most complex compounds are lacking in the literature. For the constituent molecules in the novel coronavirus, which certainly lack available optical data, the OELFs at energy losses below 40 eV were estimated by an empirical approach for bioorganic compounds developed by Tan et al. (2004a, 2004b). The OELF was expressed by the following single Drude function:

$$\mathrm{Im}[-1/\varepsilon(0, \Delta E)] = \frac{a(\Delta E)}{[(\Delta E)^2 - b^2]^2 + c^2((\Delta E))^2}, \tag{6}$$

where the parameters b and c are linearly related to the average atomic number $\bar{Z}$ of the molecule, and a can be determined by inputting the mass density of the target, the molecular weight and the total number of electrons per molecule to the f-sum rule. For energy losses larger than 50 eV, the atomic photoabsorption data of Henke et al. (1993) are available, so the OELF can be calculated from the refraction index and the extinction coefficient (Ding and Shimizu, 1996). For energy losses between 40 eV and 50 eV, the OELF was calculated by spline interpolation.

If the electron energy decreases by 2–3 times the bandgap energy during the electron cascade, the main energy-loss mechanism should be electron–phonon interactions, and the cross-section can be treated by Fröhlich's theory (Fröhlich, 1954). Low-energy electrons are also affected by the polarization field induced by their own motions through the target. This interaction is known as the polaronic effect. In this study, the cross-section of the polaronic effects was calculated by a semi-empirical approach proposed by Ganachaud and Mokrani (1995).

As shown in Fig. 1, uniformly distributed electrons with primary energies below 10 keV were irradiated over the 120-nm diameter of the novel coronavirus. The number of primary electrons was 10^5. The densities of protein, RNA and water were set to 1.3, 1.35, and

1.0 g/cm^3, respectively.

The electron trajectories were traced by two Monte Carlo strategies. The energy deposition was determined by a simple and fast Monte Carlo method based on the continuous slowing down approximation (CSDA). The CSDA assumes that electrons continuously lose energy along the electron trajectories, and change directions by elastic scattering. In the ionization-characterizing calculation, each energy loss and direction change along the electron trajectories was calculated by the energy straggling strategy. If the amount of energy lost in a single inelastic scattering event exceeded the binding energy of the atomic shell, the site became ionized, producing an inner secondary electron that was traced by the same procedure as the primary electrons (Caleman et al., 2009). This simulated electron cascade considered the events of elastic scattering, electron–electron inelastic scatterings, and electron–phonon and electron–polaron interactions (Dapor, 2014).

3. Results and discussion

3.1. OEFLs

To describe the inelastic interactions between the electrons and molecules, the OEFLs of the constituent molecules in the novel coronavirus were calculated by using Eq. (6) and atomic photoabsorption data (Henke et al., 1993), as mentioned above. The OEFL of water was adopted from Heller et al. (1974). As shown in Fig. 2, the OEFL curves of the five components peaked at energies between 20 and 25 eV. The envelope yielded the highest OEFL peak, and RNA has the maximum peak position. From the OEFLs, the probability of inelastic scattering events and the energy-loss distributions were determined.

3.2. Energy deposition

From the OELFs, the stopping power and electron-electron inelastic cross-sections were calculated by Eqs. (2)–(5). The energy deposition was investigated by the CSDA-based Monte Carlo simulation. Fig. 3 plots the energy densities deposited per unit volume (nm^3) in each shell of the novel coronavirus, as functions of the primary electron energy from 200 eV to 10 keV. Strong peaks in the energy-deposition densities appeared at primary energies of 1.5–1.7 keV. The peaks of the envelope, water, nucleocapsid, and RNA were around 1–3 keV wide, indicating that electrons with energies around 1–3 keV produce the most

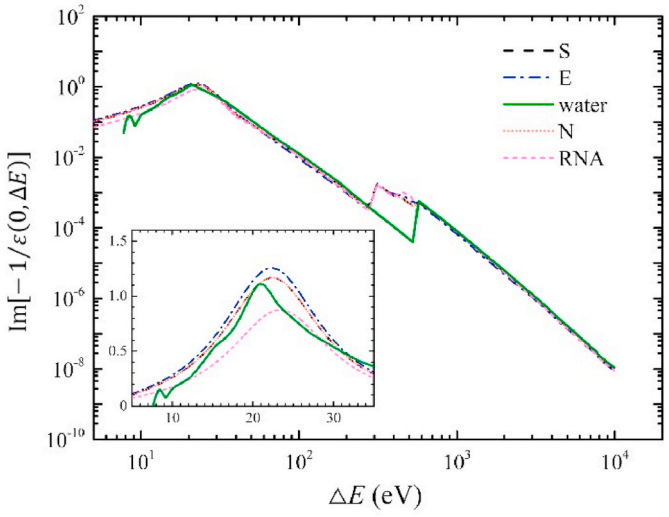

Fig. 2. Calculated optical energy-loss functions (OEFLs) of constituent molecules in the novel coronavirus: S (spike glycoproteins), E (envelope), water, N (nucleocapsid), and RNA. The OEFL of water was adopted from Heller et al. (1974).

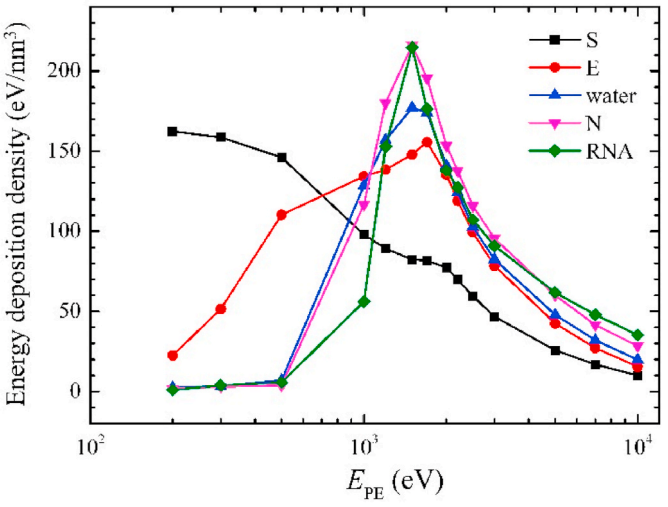

Fig. 3. Energy-deposition densities in each shell of the novel coronavirus versus energy of primary electrons.

Table 1
Total energy deposition and ionization (normalized units) in the four main components of the coronavirus (energy of primary electrons = 1.5 keV).

Component	Deposited energy (normalized unit)	Ionization (normalized unit)
Envelope	1	1
Water	0.73	0.51
Nucleocapsid	0.27	0.23
RNA	0.37	0.25

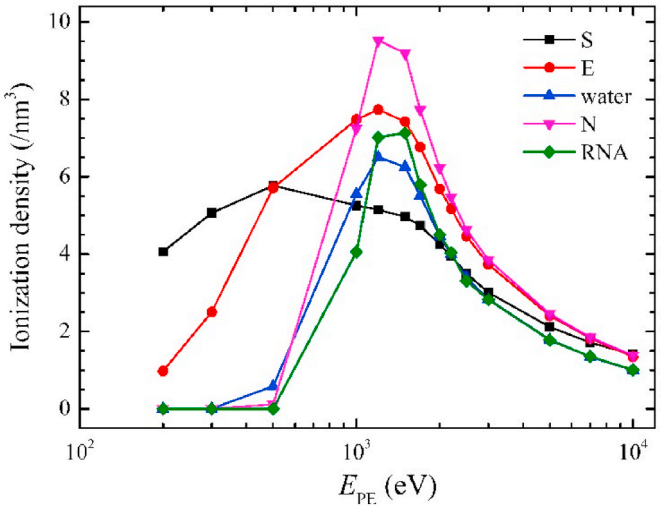

Fig. 4. Ionization densities in each shell of the novel coronavirus versus energy of primary electrons.

obvious energy transfer and deposition in the target molecules. The energy-deposition density at 1.5 keV was maximized in the nucleocapsid and RNA. Primary energies below hundreds of eV or higher than 10 keV deposit much lower energy densities in the four main shells. In contrast, the energy density deposition in the spike glycoproteins (which are sparsely spread across the outer surface) was a gently decreasing function of the primary energy. This result can be explained by the deposition of more incident electrons in the tiny outer volume of the spike glycoproteins at lower than at higher primary energies.

The total energy deposited in each main shell was obtained by multiplying the spherical shell volume and the corresponding energy-

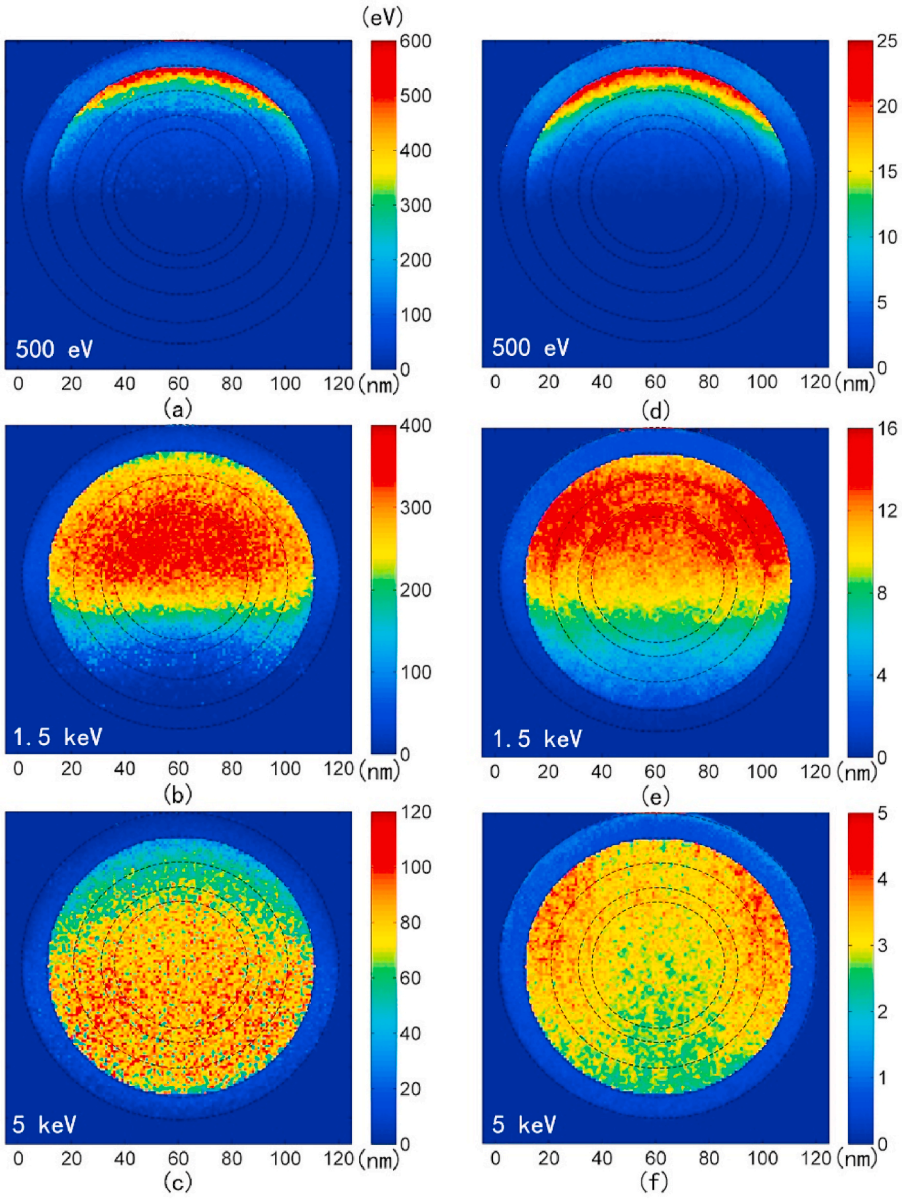

Fig. 5. Distributions of deposited energy (a)–(c) and ionization (d)–(f) through the vertical section of the novel coronavirus. The primary energies are 500 eV in (a) and (d), 1.5 keV in (b) and (e), and 5 keV in (c) and (f).

deposition density. The total energy (in normalized units) deposited by 1.5 keV primary electrons in the internal layers of the virus (from the envelope to the central RNA) are listed in Table 1. The energy deposit was maximized in the envelope.

3.3. Ionization

The inelastic scattering of the electron cascade in each component of the coronavirus was traced by the energy straggling strategy in Monte Carlo simulations. If the energy loss during a single inelastic scattering exceeds the binding energy of the atomic shell, an ionization event occurs. Each ionization event and its site were recorded. The ionization density was then computed as the number of ionization events in each unit volume (nm^3) of the target. Fig. 4 plots the ionization densities in each shell as functions of primary electron energy. Strong peaks in the ionization densities of the envelope, water, nucleocapsid and RNA shell appeared at primary energies of 1.2–1.5 keV. The ionization density was maximized in the nucleocapsid. The total ionization in each main shell (in normalized units) at the primary energy of 1.5 keV are listed in Table 1. Like the deposition energy, the ionization was maximized in the envelope. Both the energy deposition and ionization densities appeared over a larger range of primary energies (~400 eV–3 keV) in the envelope than in the other viral components (see Figs. 3 and 4).

3.4. Distribution characteristics

Fig. 5 shows the distribution characteristics of the deposited energy and ionization densities through a vertical section of the novel coronavirus. To simplify the presentation, the sparse structure of the spike glycoproteins was neglected, and the deposited energy and ionization were assumed to be uniformly distributed through the shell volume. The primary energy was varied as 500 eV, 1.5 keV, and 5 keV. At 500 eV, the energy deposition and ionization were concentrated in the upper shell (the envelope) because the penetration range of the primary electrons was small. Approximately 60% of the primary electrons lost all their energy and were deposited in the target. At a primary energy of 1.5 keV, the energy deposition and ionization covered a large part of

the cross-section. At higher energy (5 keV), over 99.9% of the primary electrons were transmitted through the coronavirus, and the energy deposition and ionization were lowered.

In this calculation model, the primary electrons vertically incident from the edge of the spherical virus will travel a slightly longer path and then lose more energy in spike glycoproteins, compared with those incident from the centre position of the shell. For example, primary electrons of 5 keV with vertical incidence from the edge are decelerated more through the spike glycoproteins, and will more likely be ionized in the next envelope shell. Thus, the ionization density was slightly raised at the edge of the envelope shell, as shown in Fig. 5(f).

Most of the electrons with energies below hundreds of eV will finally loss their energy and be deposited inside the target. As the primary energy decreases, the total amounts and densities of the energy deposition decrease accordingly. The estimated deposition depth of primary electrons with energies above 2 keV in the thick materials of the envelope, nucleocapsid, and RNA is 180 nm (Fitting, 1974), larger than the coronavirus diameter. As fast electrons have lower probability of inelastic interactions with molecules than slow electrons, their energy deposition and ionization in the target will decrease, as shown in Figs. 3 and 4. Therefore, the energy deposition and ionization densities are maximized over an optimal range of primary energies (1–3 keV). The presented results demonstrate that the characteristics of energy deposition and ionization depend on the energy loss and electron range in the coronavirus, which are mainly determined by the primary energy of the electrons. Furthermore, the electron energy deposition is correlated with the temperature rise imparted by the electron irradiation. High temperature is expected to be an important deactivating factor of the novel coronavirus.

Although electrons with lower energies (1–3 keV) effectively deposit their energies and ionize the viral macromolecules, irradiating the novel coronavirus by low-energy electrons is difficult to achieve in practice. Theoretical calculations may provide fundamental physical information on the electron irradiation of viruses.

4. Conclusions

In this paper, we performed calculations of energy deposition and ionization on the novel 2019 coronavirus by electron irradiation, using Monte Carlo methods. The electron cascade was simulated by the CSDA and the energy straggling strategy. The energy deposition and ionization densities in the main components of the coronavirus were maximized at primary electron energies of approximately 1.5 keV. At these energies, the primary electrons should largely contribute to the sterilization or inactivation effect. The correlations between the destruction of biological activity and the characteristics of energy deposition and ionization in the novel coronavirus require further investigation.

CRediT authorship contribution statement

Xiaqi Zhang: Methodology, Software, Data curation, Visualization. **Fang Wang:** Methodology, Writing - original draft, Writing - review & editing. **Ming Weng:** Writing - review & editing. **Meng Cao:** Conceptualization.

Declaration of competing interest

The authors declare that they have no known competing financial interests or personal relationships that could have appeared to influence the work reported in this paper.

Acknowledgments

This work was supported by the National Natural Science Foundation of China [Grant No. 61971342, U1537210] and the Fundamental Research Funds for the Central Universities [Grant No. xjj2017066].

Appendix A. Supplementary data

Supplementary data to this article can be found online at https://doi.org/10.1016/j.radphyschem.2020.109169.

References

Ashley, J.C., 1988. Interaction of low-energy electrons with condensed matter: stopping powers and inelastic mean free paths from optical data. J. Electron. Spectrosc. Relat. Phenom. 46 (3), 199–214. https://doi.org/10.1016/0368-2048(88)80019-7.

Benson, R.S., 2002. Use of radiation in biomaterials science. Nucl. Instrum. Methods Phys. Res. B 191, 752–757. https://doi.org/10.1016/S0168-583X(02)00647-X.

Berovic, N., Pratontep, S., Bryant, A., Montouris, A., Green, R.G., 2002. The kinetics of radiation damage to the protein luciferase and recovery of enzyme activity after irradiation. Radiat. Res. 157 (2), 122–127. https://doi.org/10.1667/0033-7587(2002)157[0122:TKORDT]2.0.CO;2.

Boudaïffa, B., Cloutier, P., Hunting, D., Huels, M.A., Sanche, L., 2000. Resonant formation of DNA strand breaks by low-energy (3 to 20 eV) electrons. Science 287 (5458), 1658–1660. https://doi.org/10.1126/science.287.5458.1658.

Caleman, C., Ortiz, C., Marklund, E., Bultmark, F., Gabrysch, M., Parak, F.G., Hajdu, J., Klintenberg, M., Timneanu, N., 2009. Radiation damage in biological material: electronic properties and electron impact ionization in urea. Europhys. Lett. 88 (2), 29901. https://doi.org/10.1209/0295-5075/88/29901.

CDC Centers for Disease Control and Prevention, 2020. https://www.cdc.gov/coronavirus/2019-ncov/index.html, Accessed date: 1 June 2020.

Chiari, L., Anderson, E., Tattersall, W., Machacek, J.R., Palihawadana, P., Makochekanwa, C., Sullivan, J.P., García, G., Blanco, F., McEachran, R.P., Brunger, M.J., Buckman, S.J., 2013. Total, elastic, and inelastic cross sections for positron and electron collisions with tetrahydrofuran. J. Chem. Phys. 138 (7), 074301. https://doi.org/10.1063/1.4789584.

Dapor, M., 2014. Transport of Energetic Electrons in Solids: Computer Simulation with Applications to Materials Analysis and Characterization, Springer Tracts in Modern Physics. Springer, Berlin. https://doi.org/10.1007/978-3-319-03883-4.

Ding, Z.J., Shimizu, R., 1996. A Monte Carlo modeling of electron interaction with solids including cascade secondary electron production. Scanning 18 (2), 92–113. https://doi.org/10.1002/sca.1996.4950180204.

Emfietzoglou, D., Kyriakou, I., Abril, I., Garcia-Molina, R., Nikjoo, H., 2012. Inelastic scattering of low-energy electrons in liquid water computed from optical-data models of the Bethe surface. Int. J. Radiat. Biol. 88 (1–2), 22–28. https://doi.org/10.3109/09553002.2011.588061.

Feng, G.B., Liu, L., Cui, W.Z., Wang, F., 2020. Electron beam irradiation on novel coronavirus (COVID-19): A Monte–Carlo simulation. Chin. Phys. B 29 (4), 048703.

Fitting, H.J., 1974. Transmission, energy distribution, and SE excitation of fast electrons in thin solid films. Phys. Stat. Solids A 26 (2), 525–535. https://doi.org/10.1002/pssa.2210260216.

Fröhlich, H., 1954. Electrons in lattice fields. Adv. Phys. 3 (11), 325–361. https://doi.org/10.1080/00018735400101213.

Ganachaud, J.P., Mokrani, A., 1995. Theoretical study of the secondary electron emission of insulating targets. Surf. Sci. 334 (1–3), 329–341. https://doi.org/10.1016/0039-6028(95)00474-2.

Heller, J.M., Hamm, R.N., Birkhoff, R.D., Painter, L.R., 1974. Collective oscillation in liquid water. J. Chem. Phys. 60 (9), 3483–3486. https://doi.org/10.1063/1.1681563.

Henke, B.L., Gullikson, E.M., Davis, J.C., 1993. X-ray interactions: photoabsorption, scattering, transmission and reflection at $E = 50$–30,000 eV, $Z = 1$–92. Atomic Data Nucl. Data Tables 54 (2), 181342. https://doi.org/10.1006/adnd.1993.1025.

Jiang, Y., Sun, J., Wan, L., 1997. Geometric shielding effects of electron scattering from polyatomic molecules. Phys. Lett. 237 (1–2), 53–57. https://doi.org/10.1016/S0375-9601(97)00813-X.

Kempner, E.S., 2001. Effects of high-energy electrons and gamma rays directly on protein molecules. J. Pharm. Sci. 90 (10), 1637–1646. https://doi.org/10.1002/jps.1114.

Kempner, E.S., 2011. Direct Effects effects of ionizing radiation on macromolecules. J. Polym. Sci. B Polym. Phys. 49 (12), 827–831. https://doi.org/10.1002/polb.22250.

Lidzey, D.G., Berovic, N., Chittock, R.S., Beynon, T.D., Wharton, C.W., Jackson, J.B., Parkinson, N.S., 1995. A critical analysis of the use of radiation inactivation to measure the mass of protein. Radiat. Res. 143 (2), 181–186. https://doi.org/10.2307/3579155.

Lu, R.J., Zhao, X., Li, J., 2020. Genomic characterisation and epidemiology of 2019 novel coronavirus: implications for virus origins and receptor binding. Lancet 395, 565–574. https://doi.org/10.1016/S0140-6736(20)30251-8.

NCBI center for Biotechnology information. https://www.ncbi.nlm.nih.gov/sars-cov-2/, Accessed date: 1 June 2020.

Nikjoo, H., O'Neill, P., Goodhead, D.T., Terrissol, M., 1997. Computational modelling of low-energy electron-induced DNA damage by early physical and chemical events. Int. J. Radiat. Biol. 71 (5), 467–483. https://doi.org/10.1080/095530097143798.

Penn, D.R., 1987. Electron mean-free-path calculations using a model dielectric function. Phys. Rev. B 35 (2), 482–486. https://doi.org/10.1103/PhysRevB.35.482.

Salvat, F., Jablonski, A., Powell, C.J., 2002. NIST Electron Elastic-Scattering Cross-Section Database. National Institute of Standards and Technology vol. 4. https://srdata.nist.gov/srd64/.

Smolko, E.E., Lombardo, J.H., 2005. Virus inactivation studies using ion beams, electron and gamma irradiation. Nucl. Instrum. Methods Phys. Res. B 236, 249–253. https://doi.org/10.1016/j.nimb.2005.04.055.

Sohrabi, C., Alsafi, Z., O'Neill, N., Khan, M., Kerwan, A., Al-Jabir, A., Iosifidis, C., Agha, R., 2020. World Health Organization declares global emergency: A review of the 2019 novel coronavirus (COVID-19). Int. J. Surg. 76, 71–76. https://doi.org/10.1016/j.ijsu.2020.02.034.

Tan, Z., Liu, W., 2014. Monte Carlo calculations of energy deposition distributions of electrons below 20 keV in protein. Radiat. Environ. Biophys. 53 (2), 427–435. https://doi.org/10.1007/s00411-014-0518-9.

Tan, Z., Xia, Y., Liu, X., Zhao, M., Ji, Y., Li, F., Huang, B., 2004. Cross sections of electron inelastic interactions in DNA. Radiat. Environ. Biophys. 43 (3), 173–182. https://doi.org/10.1007/s00411-004-0249-4.

Tan, H.Q., Mi, Z.H., Bettiol, A.A., 2018. Simple and universal model for electron-impact ionization of complex biomolecules. Phys. Rev. E 97 (3), 032403. https://doi.org/10.1103/PhysRevE.97.032403.

Tan, Z., Xia, Y., Zhao, M., Liu, X., Li, F., Huang, B., Ji, Y., 2004. Electron stopping power and mean free path in organic compounds over the energy range of 20–10,000 eV. Nucl. Instrum. Methods B 222 (1–2), 27–43. https://doi.org/10.1016/j.nimb.2004.02.017.

WHO World Health Organization, 2020. WHO statement on cases of COVID-19 surpassing 100 000. https://www.who.int/news-room/detail/07-03-2020-who-statement-on-cases-of-covid-19-surpassing-100-000, Accessed date: 1 June 2020.

Zhang, L., Tan, Z., 2010. A new calculation on spectrum of direct DNA damage induced by low-energy electrons. Radiat. Environ. Biophys. 49 (1), 15–26. https://doi.org/10.1007/s00411-009-0262-8.